International Journal of Computer Information Systems and Industrial Management Applications
ISSN 2150-7988 Volume 18 (2026) pp. 1-23

https://doi.org/10.70917/ijcisim-2026-0017
Article

A Study of Computerized Techniques for Health Monitoring and Risk Assessment of Athletes in a Big Data Environment in Sports

Xi Chen *, Yaosheng Zhang, Menglin Chen and Yuquan Shi

College of Physical Education and Health Engineering, Taiyuan University of Technology, Taiyuan 030024, Shanxi, China; cx101839@126.com

Abstract: In this study, an athlete health monitoring system based on pulse wave signals is designed to address the problems of low data prediction accuracy and poor real-time performance of traditional athlete health monitoring techniques. The system collects and preprocesses the photoelectric volumetric pulse wave signals of athletes by applying a photoelectric volumetric pulse wave acquisition sensor device. Firstly, the differential thresholding method, the pulse map area method and the waveform fitting method are used to extract the characteristic parameters in the time domain, then the power spectrum analysis and the cepstrum analysis are used to extract the characteristic parameters in the frequency domain, and the HHT method based on the time-frequency hybrid domain is also used to extract the characteristic parameters of the pulse signals. Finally, the Hidden Markov Model is introduced to convert the pulse wave signals of the athletes that need to be evaluated into a sequence of physiological signal features, and the risk assessment of the athletes' health status is carried out. The results of the study show that the system in this paper can significantly differentiate the health status of healthy and diseased populations, and the fitted curve of the recognized healthy athletes' physical health level rises by 0.065, which is in line with their actual health status level. The system in this paper provides a scientific basis for injury prevention and sports performance optimization of athletes, and has important application value in the sports world.

Keywords: pulse wave signal; photoelectric volumetric pulse wave acquisition sensor; HHT method; Hidden Markov Model; health status assessment

1. Introduction

In 1989, the World Health Organization redefined health, stating that it is not merely the absence of disease or infirmity, but rather a state of complete physical, mental, social, and moral well-being [1]. Physical education plays a significant role in the development of an individual's physical, mental, and moral well-being, and its value transfer characteristics have a positive impact on an individual's ability to adapt to society [2-3]. Therefore, physical education has a direct or indirect influence on health.

In recent years, the popularity of competitive sports has remained high, with athletes receiving significant attention. As the core force in the sports field, athletes' health status directly impacts the improvement of athletic performance, the continuation of their athletic careers, and the protection of their physical health [4-5]. With the rapid development of the sports industry, the scientific and systematic requirements for athlete health management have been increasingly emphasized. Among these, health monitoring and risk assessment of athletes, by understanding athletes' health data, developing targeted training and nutrition plans, and adjusting these plans based on real-time changes in health data, can help ensure and improve athletes' training and competition performance, prevent sports injuries, extend athletic careers, and thus promote athletes' long-term development [6-9]. As such, health monitoring and risk assessment are crucial safeguards for athletes' health, and conducting research on monitoring and

risk assessment plays an important role in promoting individual health, group health, and health management. At the same time, this also provides a strong practical basis for health management research [10-12].

In the big data environment, data research in the field of sports has undergone a revolution in research methods thanks to big data, changing the way sports are communicated and trained, giving rise to long-term development strategies for the sports industry, and enhancing the value of the sports industry [13-15]. Traditional competitive sports are relatively closed, and to maintain competitive advantages, organizers and implementers of sports training often prevent information from being disclosed. In the big data era, the environment for competitive sports has become more complex, and the application of advanced technologies enables efficient predictions, breaking the limitations of relying on traditional experience for talent selection, training, and technical analysis [16-17]. Data sensing technology, 3D Doppler radar technology, and real-time big data monitoring technology enable sports prediction and are widely applied in real-time data statistics on competition or training fields, assisting coaches in decision-making and command, and developing targeted strategies. In an information-open environment, the external environment faced by sports has become more open, diverse, and complex [18-20]. Therefore, it is necessary to leverage the information contained in big data to conduct health and risk assessments of athletes to achieve better health management.

In athlete health monitoring, literature [21] integrates multiple sensors into a new wearable system, constructing an athlete health monitor that uses wireless, real-time, and continuous advantages to monitor athletes' dehydration and physiological stress during exercise. Literature [22] combines real-time physiological and environmental data collected via wearable devices and smart terminal technology with an evolutionary difference model and an improved random forest algorithm to dynamically assess and predict athletes' health status in real time, thereby monitoring and warning of athletes' health conditions. However, this study overlooks data related to athletes' mental health. Literature [23] integrates 3D printing technology with wearable sensors to achieve real-time, personalized athlete health data collection, providing direction for athlete health monitoring in sports psychology. However, sensor interference issues remain to be addressed, and the authors suggest combining artificial intelligence with advanced biotechnology. Literature [24] developed a software system for athlete health monitoring, which involves athlete health electronic records and databases, including physical and mental health data. Literature [25] proposes the concept of covert monitoring and practical recommendations, aiming to monitor athletes' health and collect performance data without their awareness to obtain the most accurate health status. However, current covert monitoring faces multiple challenges in terms of practicality and ethics. Reference [26] mentions tools for assessing health risks in female athletes, specifically the Female Athlete Triad Alliance and Relative Energy Deficiency in Sport, which incorporate physiological data, targeted scan data, exercise and health status, and dietary survey data to determine whether athletes are fit to compete. Literature [27] employs machine learning technology to analyze athlete training, performance, and basic information data, using random forest algorithms to predict and classify injury risks, thereby assessing athletes' injury risks and contributing to injury prevention efforts.

In this study, a technical framework integrating pulse wave monitoring and athlete health risk assessment is constructed. The construction of an athlete health monitoring system based on pulse wave was realized in detail from both hardware design and software design of the athlete health monitoring system. A photoelectric volumetric pulse wave sensor is used to collect human pulse data, and the pulse signal is preprocessed with symmetric wavelet sym8. The extraction of characteristic parameters of the pulse signal is accomplished from three aspects: time domain, frequency domain and time-frequency hybrid domain. The Hidden Markov Model, which is good at dealing with state transfer features in physiological sequence data, is introduced to assess the health status of athletes. Specific cases are used to confirm the extraction effect of the pulse signal feature parameter extraction algorithm and the health risk assessment effect of athletes.

2. Design and Realization of Pulse Wave-Based Health Monitoring System for Athletes

2.1. System Hardware Design and Implementation

2.1.1. Pulse Wave Sensing Module

The pulse wave detection module adopts JFHlll intelligent health monitoring module.JFHlll pulse wave sensing module is a multi-spectrum based physiological data detection module, which can accurately detect the human body's heart rate, blood oxygen, blood pressure and vascular microcirculation and other health parameters. The module integrates signal conditioning technology and specific detection algorithms, so that the user system can communicate with the module through the

serial port and directly obtain the pulse waveform, heart rate, blood oxygen and vascular microcirculation parameters.JFHll1 module not only has an independent calculation and analysis, but also can provide more information by using “cloud” big data analysis technology, such as blood pressure trend, respiratory rate, blood pressure, blood pressure, blood pressure, blood pressure, blood vessel microcirculation, and other health parameters. The JFHll1 module provides additional information such as blood pressure trends, respiratory rate, heart rate variability, etc., in addition to stand-alone analyses.

2.1.2. Hardware Circuit Design

Controller selection STM32 and other commonly used microcontrollers, on-chip resources, complete development ecology, simple and fast design. The circuit connection of each module of the system is relatively simple, in which the communication connection between the JFHll1 pulse wave sensing module and the controller can be realized only through the UART; the system display is connected to the controller through the SPI interface; and the keys are connected to the control through the I0 port; The communication module realizes communication with the controller through the UART interface, and the communication module can be used by Bluetooth module or WiFi module to realize the wireless transmission of health monitoring data.

2.2. System Software Design and Implementation

The health monitoring system collects human pulse wave information in real time through JFHll1 sensing module, and the controller displays the pulse waveform, heart rate value, blood oxygen value and vascular microcirculation parameters on the display in real time through data processing.

The monitoring system can also wirelessly transmit the athlete's health monitoring data to the cloud health service system for heart rate variability analysis, analysis of sleep status, and monitoring of cardiovascular and cerebrovascular diseases through the Wifi module, and it can give real-time health diagnosis or improvement suggestions, or send the results to a professional doctor on a regular basis to shorten the length of time of medical treatment, so that it can be able to prevent myocardial infarction, cardiovascular and cerebrovascular diseases, and other diseases. This model allows health demanders to obtain health management services through the cloud, thus truly reducing the human and material costs of medical services, and doing a more professional and in place. Here we transfer the real-time collected pulse wave data to the cloud database as an example.

2.3. Basic Properties of Pulse Waves

The heart continuously transports fresh blood through the blood vessels to all parts of the body by contracting and diastole around the clock. When the ventricles contract and the aortic valve opens to allow blood to enter, there is resistance in the blood vessel so that some of the blood that enters the aorta is retained in the proximal part of the aorta and does not immediately enter the veins, resulting in dilatation of the aorta and an increase in blood pressure, which is visualized as a rapid and smooth rise at the beginning of the graph, known as the percussive wave, and systolic blood pressure occurs at the point of peak of the main wave. When ventricular diastole stops the entry of blood by aortic valve closure, the aorta begins to contract and recover by vascular elasticity, forming a descending branch in the graph. The flow rate of blood in the vessel changes with the heart's pacing state, as do the pressure and volume of the vessel's inner wall, and these changes propagate forward in the direction of blood flow causing the vessel to pulsate. The usual term pulse usually refers to the pulsations that people feel in the superficial blood vessels on the surface of the body.

As the pulse wave propagates outward from the aortic root along the arterial system, various parts of the arterial tree are exposed to some of the energy of the pressure wave generated by blood flow that is reflected back to the heart along the arterial system in the opposite direction. The presence of different elastic properties of the walls of different arterial segments, as well as the presence of arterial bifurcations, stenosis, etc., also results in a series of discontinuities in the arterial system. These discontinuities change the impedance of the arteries at both ends of the reflected wave, and the waveform is reflected and refracted to varying degrees at these discontinuities. Hemodynamic studies have demonstrated that pulse waves propagate in the periphery of the heart not only with centripetal reflections, but also with re-reflections at arterial valves, and because of this property, waveform variations similar to those observed for repetitive waves are observed in pulse waves. The linear combination of these recurrent pulse waves is responsible for the characteristic shape of the arterial pulse wave.

The nonlinearities of the pulse wave include the relationship of waveform characteristics and their fluctuation changes to physiopathological states, the mechanism of pulse wave formation, and kinetic modeling. The current research shows that the nonlinear effects produced by the propagation of the pulse in the arteries are mainly attributable to the nonlinear excitation of the heart, the nonlinearity of the

geometry and mechanical properties of the vascular system, the nonlinearity of the motion of the vessel walls, the nonlinear fluid peculiarities of blood flow, the complexity of the arterial vascular branching system, as well as the complexity of the propagation of the pulse.

The reflection of the pulse wave is the key influential element in determining the general shape of the arterial pulse wave. However, in reality, the change of pulse waveform is the result of the joint action of many influences, including the following aspects:

(1) Under the influence of the reflected wave, the various components of the pulse wave interact with each other, some enhancing and some canceling.

(2) Under the influence of the double damping of the blood viscosity and the elasticity of the tube wall, a certain degree of attenuation of the waveform will occur when the pulse wave propagates.

(3) The harmonic frequencies of the pulse wave are different, and their propagation speeds are also different when the frequencies are not the same, so the pulse waveform will change.

(4) Different arterial segments have different wall elasticity and arterial diameter, resulting in different propagation speeds of the pulse wave in them.

(5) Age, sex, systolic and diastolic blood pressure, and serum phospholipid levels are also important factors.

(6) As the pressure rises, the pulse wave is affected more and more by nonlinear effects.

After analyzing the generation and propagation of pulse waves and understanding their characteristics, it can be found that there are differences in the waveform characteristics of pulse waves collected from superficial arteries in different locations of the body (e.g., carotid artery, radial artery, and femoral artery, etc.). The radial artery is the most convenient peripheral vessel to detect, and it contains a variety of cardiovascular physiopathologic information, which is the first choice for pulse diagnosis. Generally, the pulse wave we often refer to is the radial artery pulse wave.

Although both pulse chart and pulse image originated from “pulse diagnosis”, their meanings are not the same, they are related to each other but not to be confused.

The cyclic contractile motion of the heart generates blood pressures that result in, among other things, constriction of the walls, which propagate peripherally into the arterial system. According to hemodynamics (blood is considered to be a fluid, so the basic principles of hemodynamics are the same as those of fluid mechanics in general) and rheological properties, when the blood pressure in the lumen of the artery changes dp , the radius of the arterial wall changes accordingly by its elasticity dr , and thus the tiny variable dp is linearly related to dr in the absence of high blood pressure:

$$\frac{dr}{r_0} = \frac{r_0}{Eh} dp \tag{1}$$

where r_0 is the radius of the vessel in its natural state, E is the Young's modulus of elasticity of the wall, and h is the wall thickness. It is therefore concluded that in the absence of severe vascular deformation, the waveform of the pressure change over time of the blood flow measured in the vessel is similar to the waveform of the change in caliber over time caused by vasodilatation and contraction. Usually we approximate the collected waveforms of changes in arterial vessel diameter over time as the waveforms of changes in blood pressure in the vessel over the same period of time.

Currently, with the support of existing technology, various sensors, such as photoelectric, piezoelectric, strain gauges, etc., are used to depict a pulsogram of the change in blood vessel diameter over time using non-invasive means, and this pulsogram is approximated to a pressure pulsogram (a waveform of a pressure pulse wave). In clinical research and application, it is difficult to accurately detect changes in the waveform of the flow pulse wave, so in general the pulsogram is considered to be a waveform diagram of the pressure pulse wave.

Pulse image in Chinese medicine is the image of pulsation should be pointed, that is, the image and dynamics of pulse beating felt by the doctor's finger when diagnosing the pulse. Including frequency, rhythm, fullness, smoothness of the situation, momentum and slow, fluctuations in the amplitude and so on. From ancient times to the present pulse classification development, there have been dozens of kinds of more.

Chinese medicine believes that the pulse is formed by the blood and gas running in the meridians, and has a close relationship with the qi and blood of the internal organs. Such as the heart of the blood, the lungs towards the hundred veins, the spleen blood, liver blood, kidney blood and other functional changes can lead to changes in the pulse, so different pulse can reflect the physiological and pathological changes in the internal organs of the qi and blood. Since ancient times, our country has utilized pulse information to diagnose human illnesses and formed a unique pulse system. Pulse information can comprehensively and objectively reflect the human body's material absorption, legend, metabolism and

other changes in the process, so pulse diagnosis can also be referred to as a diagnostic method of human body information.

2.4. Pulse Signal Acquisition and Preprocessing

2.4.1. Acquisition of pulse signals

Pulse collection device generally choose sensor, using the sensor to collect human pulse data, can quantitatively and objectively get the complete and rich information contained in the human pulse, storage and recording of pulse data, in order to facilitate the development of subsequent research and analysis work, only in contact with the human body surface, non-invasive and painless easy to be accepted by the test subjects, and easy to use the data transmission and sharing fast, therefore, in the practical application of the very widely used! Application.

In this paper, the pulse signal data acquisition system consists of photoelectric volumetric pulse wave sensors, because of the realization of the photoelectric isolation, good stability, and the sensor applies the shading finger sleeve type technology, from a large extent to the outside light interference isolation. By placing this sensor on the finger, the arterial pulse wave at the end of the finger can be measured easily and efficiently.

Measurement of human pulse wave signal specific operation process is: to ensure that the tested volunteers in the morning at 7:00 to 9:00 fasting state for the measurement, so that the tested volunteers in a sedentary state, emotional stability, smooth state, and then our photoelectric volumetric pulse wave sensor sleeve clamped to the tested volunteers in the right index finger, the sensor and the tested volunteers finger end of the good contact does not leave a gap, naturally flattened out of the collection of three minutes, the data acquisition is completed after the acquisition of pulse wave. After the data collection is completed, the collected pulse data will be automatically saved in our cell phone and then can be uploaded to the cloud or email to download the stored pulse wave data.

2.4.2. Preprocessing of Pulse Signals

Let $\Psi(t) \in L^2(R)(L^2(R)$ denote a space of square real numbers that are all productable, that is, a signal space such that the energy is fixed, and its Fourier transform [28] is $\Psi(t)$. When $\Psi(t)$ satisfies the condition:

$$C_{\Psi} = \int_R \frac{|\psi(t)|^2}{|w|} dw < \infty \tag{2}$$

When we call $\Psi(t)$ a basis wavelet or parent wavelet, we obtain a wavelet sequence by stretching and translating the parent wavelet function $\Psi(t)$:

$$\psi_{a,b}(t) = \frac{1}{\sqrt{|a|}} \psi(\frac{t-b}{a}) \tag{3}$$

where a is the expansion (scale) factor and b is the translation factor. In practical engineering applications, since $a < 0$ does not have much practical value and significance, we generally only discuss the case of $a < 0$.

For any function $f(t) \in L^2(R)$ the continuous wavelet transform is:

$$W_f(a,b) = < f, \psi_{a,b} > = \frac{1}{\sqrt{|a|}} \int_R f(t) \overline{\psi(\frac{t-b}{a})} dt \tag{4}$$

Its inverse transformation is:

$$f(t) = \frac{1}{C_{\psi}} \int_{R^+} \int_R \frac{1}{a^2} W_f(a,b) \psi(\frac{t-b}{a}) da db \tag{5}$$

The time-frequency window of the wavelet transform [29] can be adjusted by a scaling factor a and a shifting factor b. The shift factor b can change the position of the window on the phase plane time axis. The magnitude of the scaling factor b can not only affect the position of the window on the frequency

axis, but also change the shape of the window. The time-domain sampling steps of the wavelet transform at different frequencies are adjustable; at low frequencies, the wavelet transform has a lower time resolution and a higher frequency resolution: at high frequencies, the wavelet transform has a higher time resolution, while the frequency resolution decreases. When the wavelet transform is used to process the signal, the first step is to select the appropriate wavelet function to decompose the signal, then decompose the decomposed parameters into thresholds, select the appropriate thresholds to be analyzed, and finally use the processed parameters to carry out the inverse wavelet transform.

Fourier series provides a very effective function, which shows that any function with periodicity can be characterized by a function composed of a superposition of the sine and cosine functions, and the Fourier analysis with time or frequency wavelet transform is characterized by high time-frequency resolution. Therefore, it can be analyzed simultaneously in the time-frequency domain, while extracting local signal singularity characteristics. By using wavelet transform, the time domain signal noise can be effectively filtered out, while the high frequency information can be well preserved.

The first wavelet denoising method is the wavelet threshold denoising method, which is a simple but good denoising method. The larger magnitude wavelet coefficients contain most of the time domain signal energy concentrated at high frequencies. The energy of the noise corresponds to the smaller amplitude wavelet coefficients scattered among all the wavelet coefficients. According to this feature, a threshold should be set. If the wavelet coefficients are greater than the threshold, the major components of the wavelet coefficients are considered useful signals that should be retained. If the wavelet coefficients are less than the threshold, the main components of the wavelet coefficients may be contaminated by noise that should be eliminated. This will achieve the purpose of denoising. The key step in wavelet threshold denoising is how to select and process the threshold.

For this paper, the one-dimensional pulse signal denoising process can be divided into three steps, and the detailed steps are shown in Figure 1.

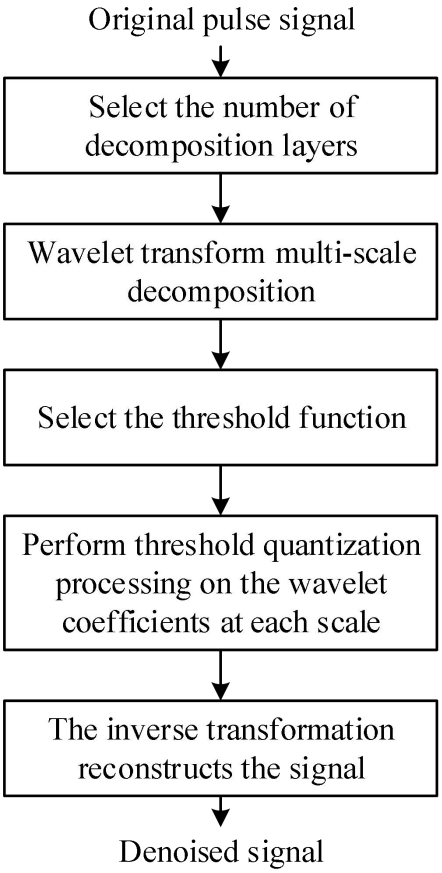

Figure 1. Noise reduction process of one-dimensional pulse signal.

In the above steps, the most important thing is how to choose a suitable threshold. Because he determines the quality of the denoising of the pulse wave signals that we collect from some extent. There are also three methods for this step as follows:

(1) Forced threshold denoising: set all the high-frequency coefficients in the wavelet decomposition

process to 0. This means that all the high-frequency parts are forced to zero filtering. The signal is then reconstructed. Although this method is simple and the reconstructed signal is smoother, it will also filter out some useful information of the signal.

(2) Default threshold denoising: for a one-dimensional pulse time-domain signal, the default threshold can be calculated using this formula:

$$thr = \frac{\sqrt{2\ln n} \times m}{0.6745} \tag{6}$$

(3) Soft or hard threshold denoising: for a given soft threshold or hard threshold denoising, in fact, the thresholds are often obtained by empirical formulas and can be more reliable than the default threshold.

Denoising experiments have been performed on the raw pulse signal, and it is clear that forced denoising filters out all the high-frequency part, including some useful information, the shape of which has been changed. The default threshold is generated by the system and coefficients smaller than the threshold are eliminated. Theoretically, the third method is better than the first two because the wavelet coefficients at all levels have different thresholds. So in this paper, the default threshold denoising is finally chosen. But at the same time, more work and experience is needed to try the thresholds corresponding to the individual wavelet coefficients. Compare the results of different wavelets. Finally, the almost symmetric wavelet sym8 is used to remove the pulse signal noise.

2.5. Algorithm for Extracting Characteristic Parameters of Pulse Signal

2.5.1. Time Domain Feature Parameter Extraction Algorithm

It is an intuitive and effective time-domain analysis method to extract some characteristic parameters with clear physiological significance through the pulse map, which mainly includes the differential threshold method, the pulse map area method, and the waveform fitting method.

The characteristics of the pulse waveform are mainly manifested in the extreme points and inflection points of the waveform, so the extraction of the characteristic parameters of the pulse can be easily realized by using the differential threshold method.

The first-order and second-order differentiation of the pulse signal can be processed to obtain the maximum value point of the signal. Since the height of the main wave of the pulse signal is the maximum value point in one cycle, a better recognition effect can be obtained by adjusting the value of the parameter m by setting the maximum value of the signal whose height is greater than m times. Similarly, a better recognition effect can be obtained by setting the maximum value of the heavy beat wave height greater than n times less than m times.

Through the transformation law of the first-order and second-order differential signal, the point of signal minima is found, and when the setting of the height of descending middle isthmus is greater than k times the maximum value of the signal, a better effect of feature parameter extraction can be obtained. Meanwhile, observing the collected pulse signal, it can be seen that the pulse signal has more distribution of very small value points around the starting point, and it is easy to introduce confusion and unable to accurately distinguish the feature point when the differential threshold method is used for the location information extraction of the point. And when the first-order differential value of the point is required to be greater than a specific value a, better results can be obtained.

The pulse waveform eigenvolume K value based on the area of the pulse map assumes that when the peripheral vascular resistance and the degree of hardening of the vascular wall, etc., change, the pulse waveform will change, which will lead to a change in the K value. At the same time, some blood flow parameters can also be calculated and derived using the K -value, therefore, the K -value can be considered as an important pulse characterization parameter. It is defined as:

$$K = \frac{Q_m - Q_{\min}}{Q_{\max} - Q_{\min}} \tag{7}$$

Or:

$$Q_m = Q_{\min} + K(Q_{\max} - Q_{\min}) \tag{8}$$

where $Q_m = \frac{1}{T}\int_0^T Q(t)dt$ refers to the average blood flow of the volumetric pulse waveform,

$Q(t)$ is the volumetric pulse blood flow curve, $Q_{\max}, Q_{\min}$ refer to the maximal and minimal values of the blood flow curve, respectively, and T is the volumetric pulse cardiac cycle.

According to the structural characteristics of the pulse waveform, the pulse waveform can generally be regarded as a superposition of several major waveforms, and the fitting function can be obtained by selecting a suitable base waveform and curve fitting the pulse waveform to maximize the proximity of the discrete data points to the fitting function, which is obtained by this process. In turn, the characteristic parameters of the pulse signal can be obtained through the fitting function.

Based on the photoelectric volume pulse signal characteristics, it is considered to be a superposition of n Gaussian functions with the following expression:

$$x(t) = \sum_{i=1}^{n} V_i o \exp\{-\frac{(t-T_i)^2}{U_l}\} \tag{9}$$

The TPS model represents the original acquired signal $p_a(t)$ as a superposition of the forward wave $p_b(t)$ and the reflected wave $p_c(t)$, and both the forward wave and the reflected wave are simulated in the form of a Rayleigh function, which is expressed as follows:

$$p_b(t) = (\alpha_b) \times (\frac{t}{\sigma_b^2}) \times \exp(-\frac{t^2}{2 \cdot \sigma_b^2}), t \geq 0 \tag{10}$$

$$p_c(t) = \begin{cases} 0 & 0 \leq t \leq D \\ (\alpha_c) \times (\frac{t-D}{\sigma_c^2}) \times \exp[-\frac{(t-D)^2}{2 \cdot \sigma_c^2}] & D < t \leq T \end{cases} \tag{11}$$

Therefore, the fitted waveform $p_d(t)$ can be obtained as:

$$p_d(t) = p_b(t) + p_c(t) \tag{12}$$

where T is the pulse period, which can be obtained by waveform fitting to obtain the forward wave height p_1, the reflected wave height p_2, the forward wave peak position $\iota p_1 = \sigma_b$, the reflected wave peak position tp_2, the peak-to-peak interval $\Delta t_T PS = tp_2 - tp_1$, reflection index $RI_T PS = p_2 / p_1$, pulse transmission time D, and time-domain difference between propagation time of advancing and reflected waves $DPS = \sigma_b - \sigma_c$. parameters. These parameters are then statistically analyzed to obtain their effects on the pulse signal and to determine the connection between this parameter and the parameters of the cardiovascular system. Based on the TPS model waveform fitting and the relationship between the fitted parameters and the cardiovascular system need to be further studied in depth.

2.5.2. Frequency Domain Feature Parameter Extraction Algorithm

Through the fast Fourier transform, the time-domain signal is transformed to the frequency domain, and the corresponding amplitude spectrum, phase spectrum, power spectrum and energy spectrum and other information are obtained, which is an important method of extracting the characteristic parameters in the frequency domain. It mainly includes power spectrum analysis and cepstrum analysis.

Using Fourier transform, the time domain signal $x(t)$ can be transformed to the frequency domain:

$$X(f) = \int_{-\infty}^{+\infty} x(t) e^{-j2\pi ft} dt \tag{13}$$

Similarly, the frequency domain information can be transformed to the time domain by Fourier inverse transform to get

$$x(t)=\frac{1}{2\pi}\int_{-\infty}^{+\infty}X(f)e^{j2\pi ft}df \tag{14}$$

The Fourier transform of the acquired pulse signal can be used to obtain the Fourier spectrum containing phase and amplitude information, and the amplitude can be obtained by the abs function in Matlab, which intercepts signals within the frequency range of 20 Hz.

Similarly, the phase spectrum of the signal can be obtained from the angel function in matlab. The power spectrum can be obtained by squaring the amplitude spectrum, and then the energy spectrum can be obtained by integrating the power spectrum in a specific frequency range.

The power spectral density $S(f)$ is defined as:

$$S(f)=\frac{2}{T}\times X(f)\times X^{*}(f)=\frac{2}{T}|X(f)|^{2} \tag{15}$$

where $X^{*}(f)$ refers to the complex conjugate of $X(f)$.

Further, the energy values in the frequency range f_1 to f_2 are obtained as:

$$E_{f_1-f_2}=\int_{f_1}^{f_2}S(f)df \tag{16}$$

Similarly, the ratio of the total energy accounted for by the energy of the $0-n$ Hz signal can be obtained, i.e., the power spectrum energy ratio:

$$PSER(n)=\frac{E_{0-n}}{E_{0-f_{\max}}}=\frac{\int_0^n S(f)df}{\int_0^{f_{\max}}S(f)df} \tag{17}$$

In addition to this, we can obtain the spectral energy ratio of the total energy accounted for by each main peak frequency, i.e., the energy ratio of each harmonic component p_i, which is:

$$p_i=\frac{\int_{f_a}^{f_b}S(f)df}{\int_0^{f_{\max}}S(f)df} \tag{18}$$

The cepstrum is obtained by taking logarithm of the spectrum and then performing inverse Fourier transform, which transforms the periodic signal in the frequency domain into a single line spectrum on the cepstrum and its inverted harmonics in order to accurately extract the period of the pulse signal through the characteristics of the inverted harmonic peaks. The purpose of taking logarithms is to multiply the different sizes of peaks in the spectrum by different multiples to enhance the smaller peaks and reflect the characteristic differences between different signals more obviously.

$$C(\tau)=F^{-1}\{10\log S(f)\} \tag{19}$$

where $F^{l}\{\}$ denotes the Fourier inverse transform.

2.5.3. Time-Frequency Hybrid Domain Feature Parameter Extraction Algorithm

Like the wavelet transform, the HHT transform can also obtain the time and frequency domain characteristic parameters of the pulse signal. The following is mainly an example of extracting energy feature parameters:

(1) Energy feature parameter extraction based on EMD method

After the original pulse signal is decomposed by EMD, a number of IMFs and a residual component can be obtained, which are denoted as $c_1(t),c_2(t),c_3(t),\cdots\cdots,c_n(t)$, where $c_n(t)$ is the residual component. Based on these parameters, the energy value of each IMF component can be obtained:

$$E_i=\int_{-\infty}^{+\infty}|c_i(t)|^2dt,i=1,2,\cdots,n \tag{20}$$

So the total energy value of the IMF component is:

$$E = \sum_{i=1}^{n} E_i \tag{21}$$

This leads to a normalized energy of:

$$T_i = \frac{E_i}{E} \tag{22}$$

At the same time, the concept of modal energy quotient is introduced in order to exclude the influence of the respective characteristics of the signals on the calculation results:

$$R_{(i*j)/(h\mathring{a}k)} = \frac{T_i + \cdots + T_j}{T_h + \cdots + T_k} \tag{23}$$

Selecting a specific i, j, h, k will give some stability to the energy quotient.

(2) Energy feature parameter extraction based on Hilbert spectrum

EMD decomposition of the pulse signal and omitting the residual error $r_n(t)$ can be obtained:

$$x(t) = RP\sum_{i=1}^{n} a_i(t)e^{j\theta_i(t)} = RP\sum_{i=1}^{n} a_i(t)e^{j\int w_i(t)dt} \tag{24}$$

where RP denotes taking the real part. The expansion of the above equation is the Hilbert spectrum, i.e.,:

$$H(w,t) = RP\sum_{i=1}^{n} a_i(t)e^{j\int w_i(t)dt} \tag{25}$$

In turn, the boundary spectrum can be obtained:

$$h(w) = \int_0^t H(w,t)dt \tag{26}$$

At the same time, there is according to the theorem of conservation of energy:

$$\int_{-\infty}^{+\infty} |\, x(t)\,|^2 \, dt = \int_{-\infty}^{+\infty}\int_{-\infty}^{+\infty} H^2(w,t)dwdt \tag{27}$$

where $H^2(w,t)$ denotes the energy spectrum, which in turn leads to the marginal energy spectrum $E(w)$, and the marginal energy spectrum $E(w)$ describes the distribution of signal energy with frequency. It is defined as:

$$E(w) = \int_{-\infty}^{+\infty} H^2(w,t)dt \tag{28}$$

Similarly, from the marginal energy spectrum, the normalized spectral energy of the signal in the frequency range w_1 to w_2 is obtained:

$$T_i = \frac{\int_{w_1}^{w_2} E(w)dw}{\int_{-\infty}^{+\infty} E(w)dw} \tag{29}$$

HHT extracts the energy characteristic parameters with the wavelet transform, which also obtains the normalized energy distribution of the pulse signal, and the specific calculation process will not be described in detail.

3. Hidden Markov Model-Based Health Risk Assessment for Athletes

3.1. Basic Theory of HMM

Hidden Markov Models (HMM) [30] are currently widely used in the fields of speech recognition, natural language processing and pattern recognition. HMM is a mathematical model based on Markov chains. Generally, the problems solved using HMM have these two characteristics:

(1) The problem is based on sequences, e.g., time series, state sequences, etc.

(2) There are two kinds of data in the problem, one kind of data can be observed as observation sequence, and the other kind of data cannot be observed as state sequence, i.e. "hidden state".

A problem that has both of these characteristics can generally be solved using an HMM model. For example, when typing on a computer using a keyboard, the series of characters typed is a sequence of observations. And a sentence you want to write in your head is the hidden sequence, and the task of the input method is to convert the series of characters typed on the keyboard into a sentence you want to express in your head. In addition to areas such as pattern recognition, it can also be applied to partially simple problems. An HMM model can be described by the following parameters:

(1) N: the number of states of the Markov chain in the model. Denote the N states as $S_1, S_2, ..., S_N$, and remember that the state in which the Markov chain is in at the moment t is q_t, and it is obvious that $q_t \in (s_1, s_2, ..., s_N)$.

(2) M: A hidden state the number of kinds of observations it produces. Denote M observations as $o_1, o_2, ..., o_M$.

Denote the observation at the moment t as o_t, where $o_t \in (o_1, o_2, ..., o_M)$.

(3) π : initial probability distribution vector, $\pi = (\pi_1, \pi_2, ..., \pi_N)$. The probability that the model is in this state at the initial moment of π_N. Among them:

$$\pi_i = P(q_i = s_i), 1 \le i \le N \tag{30}$$

(4) A: State transfer matrix, $A = \{a_{ij}\} N * N$. Among them:

$$a_{ij} = P(q_i + 1 = s_i \mid q_i = s_i), 1 \le i, j \le N \tag{31}$$

(5) B: Probability matrix of observations, $B = \{b_{jk}\} N * M$. where:

$$b_{jk} = P(o_i = v_k \mid q_i = s_j), 1 \le j \le N, 1 \le k \le M \tag{32}$$

In this way, the HMM can be written as $\lambda = (N, M, \pi, A, B)$, because in the model, the individual parameters are in turn related in some way, and A and B can only be computed after N and M have been determined, so the HMM can be abbreviated as $\lambda = (\pi, A, B)$.

According to the above definition of HMM, the set of observations is:

$$V = \{\text{red,white}\}, M = 2 \tag{33}$$

The set of states is:

$$Q = \{\text{Box No. 1;Box No. 2;Box No. 3}\}, N = 3 \tag{34}$$

In this HMM model, the length of the observation sequence and the state sequence is 3.

The initial state distribution is:

$$\pi = (0.2, 0.4, 0.4)^T \tag{35}$$

The state transfer probability distribution matrix is:

$$A=\begin{bmatrix}0.5 & 0.2 & 0.3\\ 0.3 & 0.5 & 0.2\\ 0.2 & 0.3 & 0.5\end{bmatrix} \tag{36}$$

The probability matrix of the observed sequence is:

$$B=\begin{bmatrix}0.5 & 0.5\\ 0.4 & 0.6\\ 0.7 & 0.3\end{bmatrix} \tag{37}$$

The probabilistic theoretical basis of the HMM model is the Markov chain, but the HMM is more complex.The main difference between the HMM model and the Markov chain model is that in the Markov chain, all states can be directly observed, whereas in the HMM model, the hidden states are not observable, but can only be inferred from the sequence of observations.There are two stochastic processes included in the HMM, one is the random appearance of the sequence of observations, and the other is the random transition of the hidden states. The other is the random transition of the hidden state.

3.2. Model Training and Evaluation

For the assessment of athletes' health risk, this paper proposes to complete the data analysis based on the Hidden Markov Model (HMM), which is widely used in most of the state prediction assessment. In the health risk assessment of athletes, the HMM is utilized to participate in the training, and the hidden variable that exists in the health monitoring system in a certain time period is set as q_t, which represents the implied state at the moment of t, which cannot be obtained by direct observation, and since each state tends to a different state, it is represented by the set $S=\{S_1,S_2\cdots S_N\}$. It is measured that there are m monitoring states of the health monitoring system in a given time period, and each change in the state data of the series depends on the previous state as $Q_1,Q_2\cdots Q_N$, where the initial state is denoted as Q_0. According to the probability distribution of the Hidden Markov Model with an implied state at the initial moment is π, in the Hidden Markov Model, whose state at any moment is K_i, and the next state is K_j, the probability of the state transfer can be recorded as A. If the state is K_j, the observation value is R_s, and the output observation can be recorded as value probability is B, then the model can be written as $\lambda=(\pi,A,B)$. The training model firstly computes the given model λ and the observation sequence P, and secondly the observation sequence is learned under maximum likelihood to derive its maximum probability, and the current state is obtained by matching.

The model parameters $\lambda_k=(\pi,A_k,B_k)$ corresponding to the athlete's healthy state are obtained from the training sample data respectively, as well as the model parameters of the state model $\lambda_q=(\pi,A_k,B_k)$ corresponding to the health risk state. When evaluating, the human physiological signals to be evaluated are converted into corresponding feature sequences, and then substituted into the two models trained above for probabilistic evaluation, and the one with significantly larger probability is the result of the athlete's current health risk assessment.

4. Results of Extracting Characteristic Parameters of Pulse Signals

4.1. Time-Domain Analysis of Pulse Signals

Clinical medicine indicates that older athletes have blood concentrations, degree of vascular elasticity, and peripheral vascular resistance profiles similar to those of patients with cardiovascular disease. The next task is to determine whether time domain analysis can distinguish between these two groups. Observing a set of pulse waveforms, Fig. 2's (a) and (b) show the pulse wave signals of a 50-year-old athlete and a 55-year-old hypertensive patient, respectively, measured at rest.

The two waveforms have common features: feature points are not prominent, the cutoff is flat, and the main wave is wide. Obviously, the way of finding waveform feature points in the time domain is not suitable for analyzing this kind of pulse signals with ambiguous pulse map features. In order to better reflect the differences in the time-domain characteristics of the pulse signals, this paper calculates the

pulse eigenvalues K of the two, the K value of the former is 0.395, and the pulse is a high-resistance chordal pulse; the K value of the latter is 0.404, and the pulse is a high-resistance chordal pulse with astringent veins, and there is no obvious difference in the size of the K value.

In summary, although the time-domain feature parameter can, to a certain extent, reflect the real-time changes in the degree of arterial vascular sclerosis and blood viscosity with age, the method identifies a single feature point and characterizes limited human physiopathological information, and it cannot determine whether it is the age increase or the change in pathological information. Further analysis of the frequency domain characteristics of the pulse signal is needed.

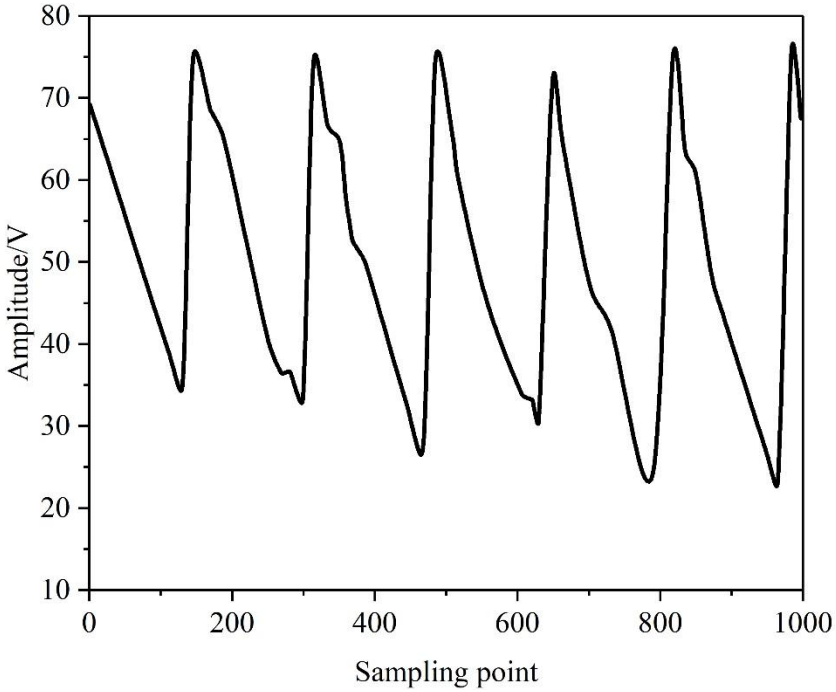

(a) Pulse wave signal of 50 years old

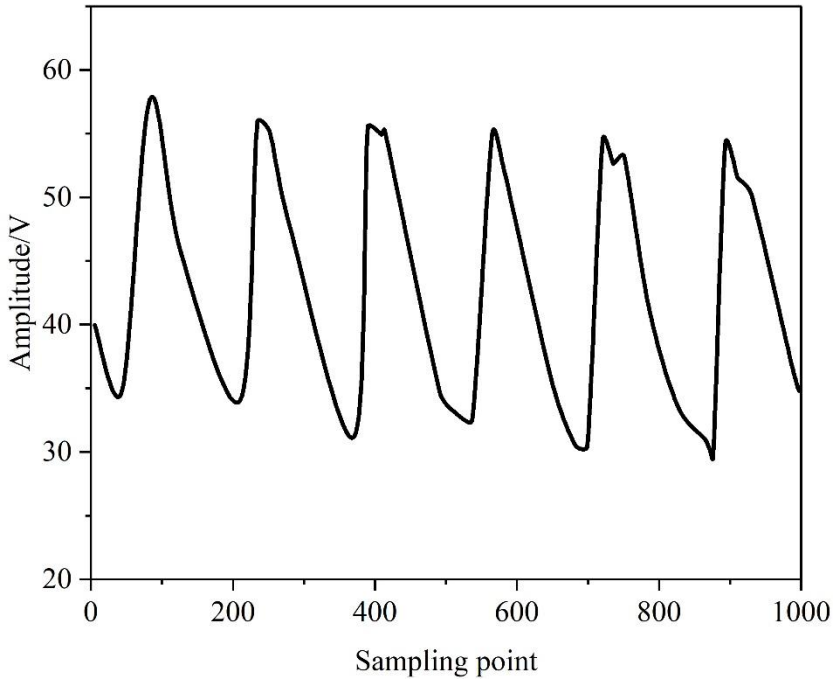

(b) Pulse wave signal for patients with hypertension

Figure 2. Pulse waveform of elderly athletes and hypertension patients.

4.2. Example Analysis of Frequency Domain Features

The spectrogram can be obtained by performing FFT variation on the pulse signal. Figures 3 and 4 show the pulse signals of a young man and a middle-aged woman and their spectrograms, (a) and (b) show the pulse waveforms and spectrograms of the subjects, respectively. From the figure, it can be seen that the pulse frequencies of both subjects are centrally distributed between 0 and 13 Hz, and the energy amplitude of the first main peak harmonic is the largest. The frequency of the main peak is close to the fundamental frequency of the human heart vibration system; the sub-harmonics after the first main harmonic are more neatly distributed, with decreasing amplitude, and the horizontal coordinate of each harmonic represents the vibration frequency of the human heart, liver, kidneys, lungs, spleen, stomach and other organs, respectively. It is calculated that the heart rate of young men at this time is about 71 beats/min, the heart rate is in the normal range, combined with the time domain analysis is judged to be normal pulse. The heart rate of a middle-aged woman is about 61 beats/minute, which is on the slow side, and the pulse is judged to be a Late Pulse by combining the time domain analysis.

It has been clinically proven that with changes in the body's pathological information, changes in blood viscosity and the degree of elasticity of blood vessels can affect the distribution of pulse frequency. Scientists use the spectral characteristics of the pulse signal to derive the pulse frequency distribution of healthy people and patients with coronary heart disease, the latter is reflected in the spectrogram as a more dispersed frequency distribution, there is still a distribution above 20Hz, and the amplitude of the first harmonic is not necessarily the largest. The spectral characteristics of the pulse signal directly reflect the frequency range of the human pulse and the speed of the heart rate, which is the simplest and most intuitive way to distinguish between healthy people and people with cardiovascular diseases. However, the spectrum obtained by FFT contains many harmonic components that are not related to the signal, and the frequency characteristic information is too single, which only reflects the change of heart rate and cannot determine the patient's disease, and it is necessary to further map the signal in the time-frequency domain to analyze the energy distribution characteristics of the pulse signal.

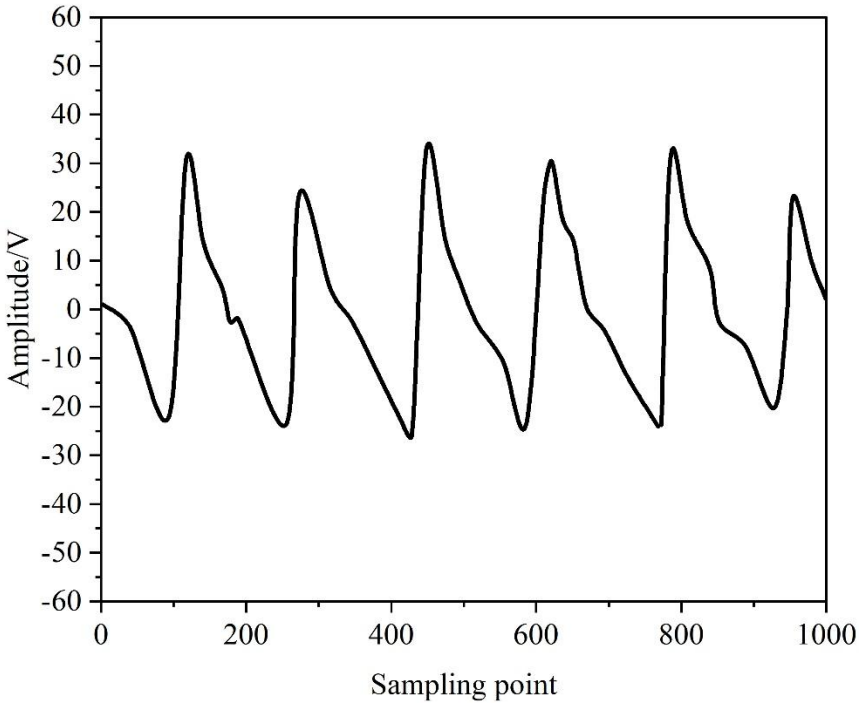

(a) The subjects' pulse

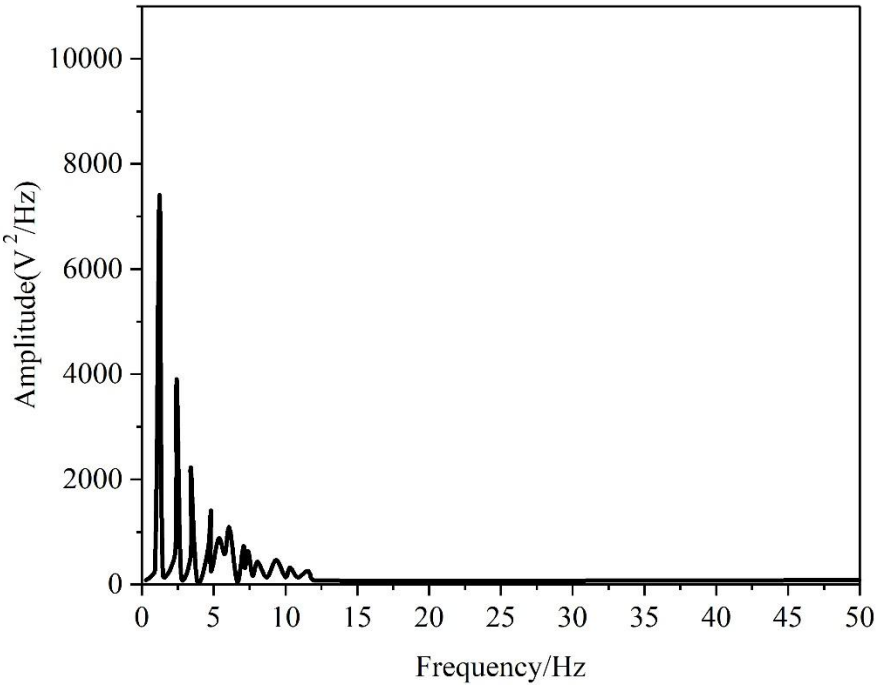

(b) Subject spectrum

Figure 3. Young men test results.

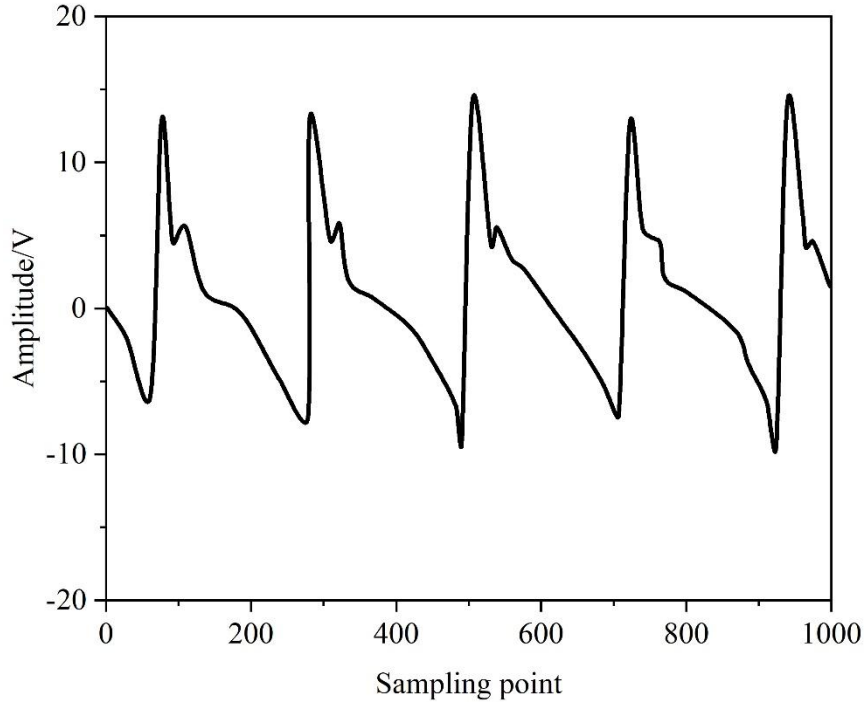

(a) The subjects'

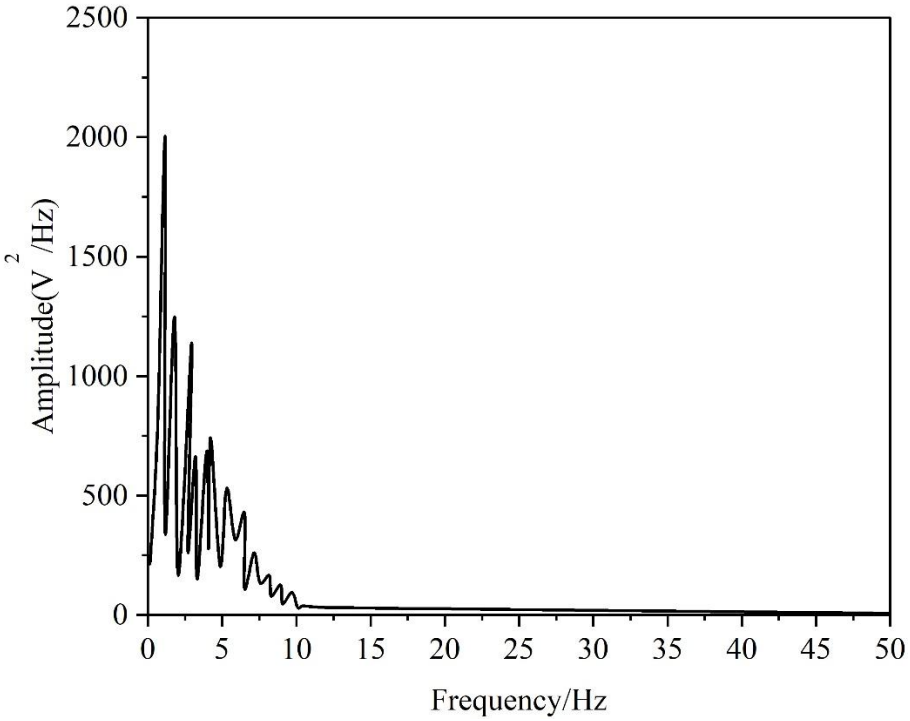

(b) Subject spectrum

Figure 4. Middle-aged women test results.

4.3. Time-Frequency Domain Analysis of Pulse Signals

Based on the feature extraction process of HHT marginal spectral energy, the pulse signals of a healthy person and a patient with coronary artery disease were decomposed by EMD respectively, and the differences between patients with coronary artery disease and the healthy population were analyzed from the distribution of the HHT marginal spectra and the mean square deviation of the energy of the two types of signals.

The total HHT marginal spectra were analyzed for both pulse signals, and the results of the HHT total marginal spectra analysis are shown in Figure 5, with the marginal spectra of pulse signals from healthy people and patients with coronary artery disease shown in Figures (a) and (b), respectively.

The HHT marginal spectrum is the result of summarizing the Hilbert spectra of the IMF components of each layer together, and compared with the FFT spectrogram, there are many fewer high harmonic components and the amplitude of the frequency is greatly reduced. The frequency distribution of the marginal spectrum of healthy people is very concentrated, usually between 0 and 11 Hz, while the marginal spectrum energy of patients with coronary artery disease still has more distribution above 11 Hz than that of the healthy population, the amplitude of the main frequency is significantly lower than that of the healthy people, and the width of the main frequency is also significantly wider than that of the healthy people. Therefore, the energy distribution of the marginal spectrum can be used as an important basis for diagnosing the cardiovascular health status of human beings. Analyzing the difference between the HHT spectra of the two types of pulse signals does not have high applicability, and in order to be intuitive and easy to understand, this paper decomposes the pulse signals of five healthy people and five patients with coronary artery disease by EMD respectively, and calculates the marginal spectral energy ERi of each layer of IMF and its rms deviation, in order to find the characteristic parameter that can directly differentiate between the two types of populations.

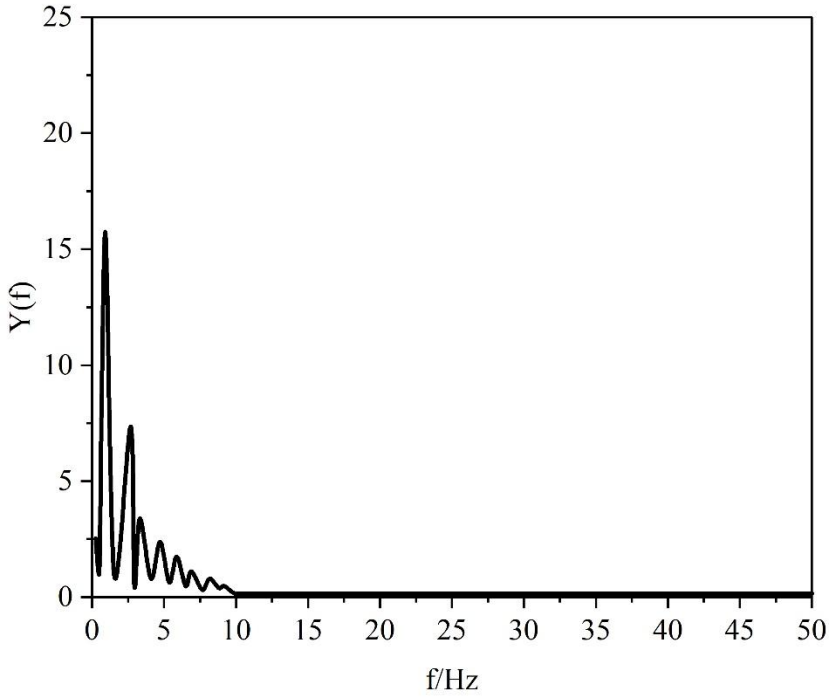

(a) The current pulse signal of a healthy person

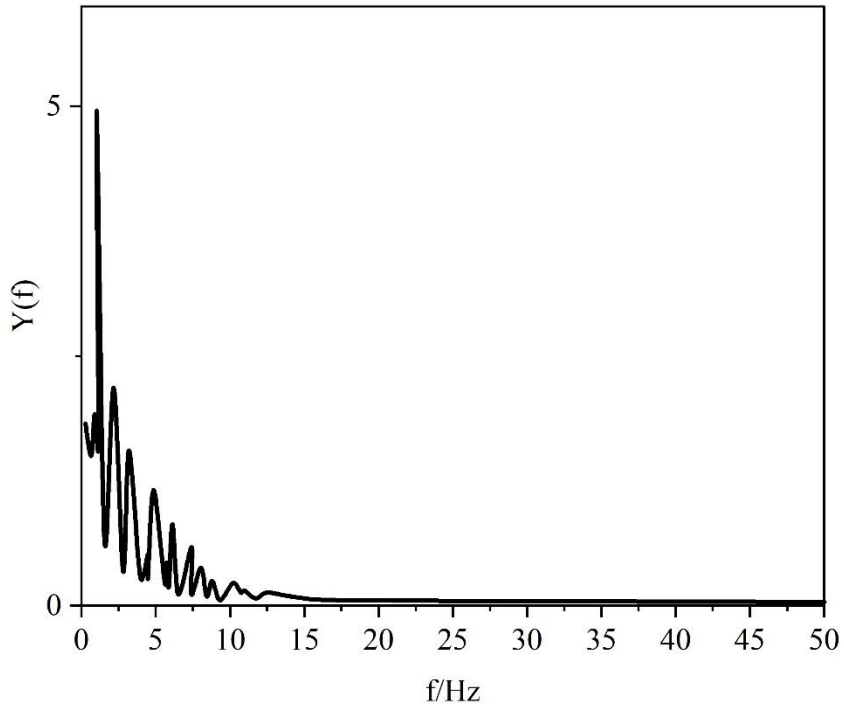

(b) The marginal graph of the pulse signal of patients with coronary heart disease

Figure 5. HHT total marginal spectral analysis results.

Tables 1 and 2 show the results of calculations for some healthy people H and patients with coronary artery disease M, respectively. The data in the tables reflect that the marginal spectral energies of patients with coronary artery disease and the healthy population show an irregular distribution on the IMF1~IMF7 components, so the mean square deviation of the energies of the IMFs in each layer was taken to explore the differences between the two populations in terms of the degree of dispersion of the energy distribution.

The marginal spectral energies of patients with coronary artery disease were distributed below 1% on more IMF components, and the maximum energy exceeded 80%, and the mean squared deviations were

all higher than 20, indicating a large degree of dispersion in the energy distribution of each layer; however, the energies of the healthy population had maximum energies of no more than 50% on the IMF1-IMF7 components, and the mean squared deviations were lower than 17, indicating a small degree of dispersion in the distribution of the energies of each layer. The conclusion that the marginal spectral energy distribution is more dispersed in patients with coronary artery disease and concentrated in healthy people is further verified. Through a large number of experiments, it is proved that the mean square deviation of the marginal spectral energy of IMFs in each layer can be used as the characteristic information to distinguish between patients with coronary artery disease and healthy people, and it can play a better effect on the monitoring of the health state of athletes, and accurately distinguish between athletes in the diseased state and those in the healthy state.

Table 1. Marginal spectral energy and mean square error of IMFs in each layer.

Healthy man	ER1	ER2	ER3	ER4	ER5	ER6	ER7	Mean variance
H1	22.5568	40.9846	8.3595	0.1435	22.0870	3.3675	2.5016	13.8108
H2	2.75240	3.1200	16.3289	51.2990	19.0009	6.7325	0.7666	16.4483
H3	42.9081	10.1578	27.6631	3.5972	11.1769	3.1735	1.3235	14.2955
H4	22.1163	47.6291	7.0155	18.8124	3.3643	0.5515	0.5125	15.7841
H5	0.4896	0.2236	3.4764	19.0268	22.1526	14.9801	39.1000	13.1225

Table 2. Marginal spectral energy and mean square error of IMFs in each layer.

Coronary heart disease	ER1	ER2	ER3	ER4	ER5	ER6	ER7	Mean variance
M1	81.3954	4.6184	0.1970	10.3284	0.3222	0.5891	0.5493	27.7298
M2	12.5887	8.2017	76.5615	0.4666	0.9888	0.1840	0.0082	26.5068
M3	1.2121	83.7006	4.5384	1.0587	4.5429	1.0106	3.9381	28.3795
M4	0.1065	0.4910	3.9205	7.7254	7.3396	18.9977	61.4191	20.1201
M5	0.0234	5.6981	9.5691	81.0713	3.6374	0.0013	0.0000	27.4682

5. Analysis of the Effectiveness of Health Risk Assessments for Athletes

The first set of data came from a 30-year-old retired athlete who was tested over a period of 20 days. At the beginning of the test, the retired athlete was free of any illness and remained in good health, but at a later stage, the retired athlete suffered from a cold that continued to worsen. The physiological data collected by the mattress was saved in csv file format, which included respiratory signal, heartbeat signal, and four physiological parameters of heart rate variability, respiratory rate, mean pressure, and heart rate. the four physiological parameters were extracted from the raw signal by the data acquisition front-end. The amount of raw data is too large and the performance is disorganized, which leads us to be unable to identify the health change status of the tester. Therefore, the signal needs to be further analyzed.

The different feature sets are projected into three-dimensional space to draw the human health status change curve, which is shown in Fig. 6, and (a) to (c) show the results based on 38 original features, the results based on 4 normal physiological features, and the results based on 42 new original features, respectively.

The analysis of the changes in the fitted curves shows that the degree of decline in graphs (a), (b) and (c) is 0.187, 0.263 and 0.328, respectively. The overall trend change of the three graphs is downward, and the change is obvious. From the analysis of the results, it can also be learned that the trend of change is more significant for the results obtained by fusing 38 signal features with 4 physiological features compared to the results obtained by 38 features with 4 physiological features. This is because the more features are fused, the more complete the human physiological information contained, and the results obtained will be more accurate.

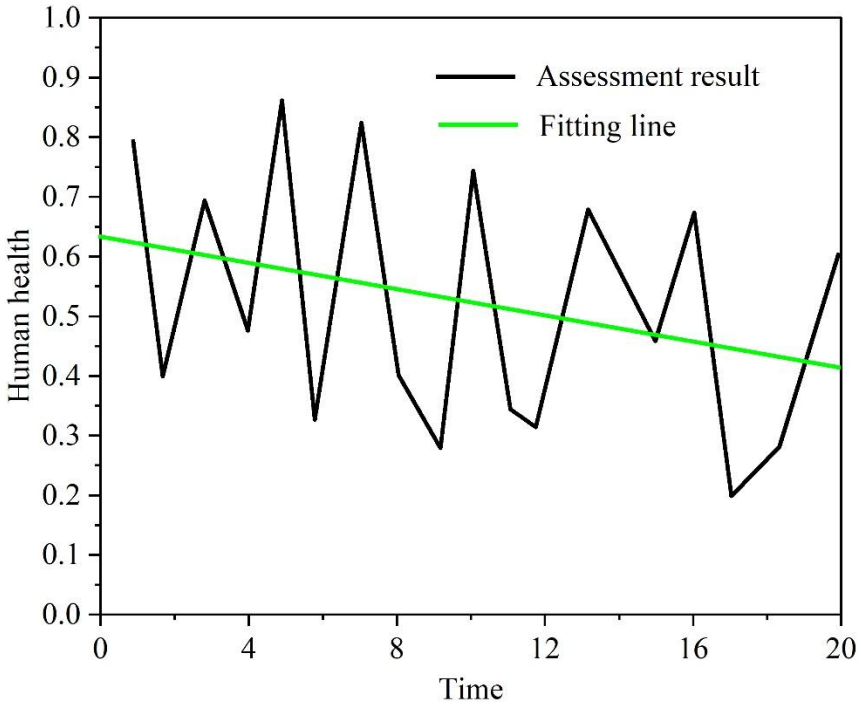

(a) Results based on 38 primitive features

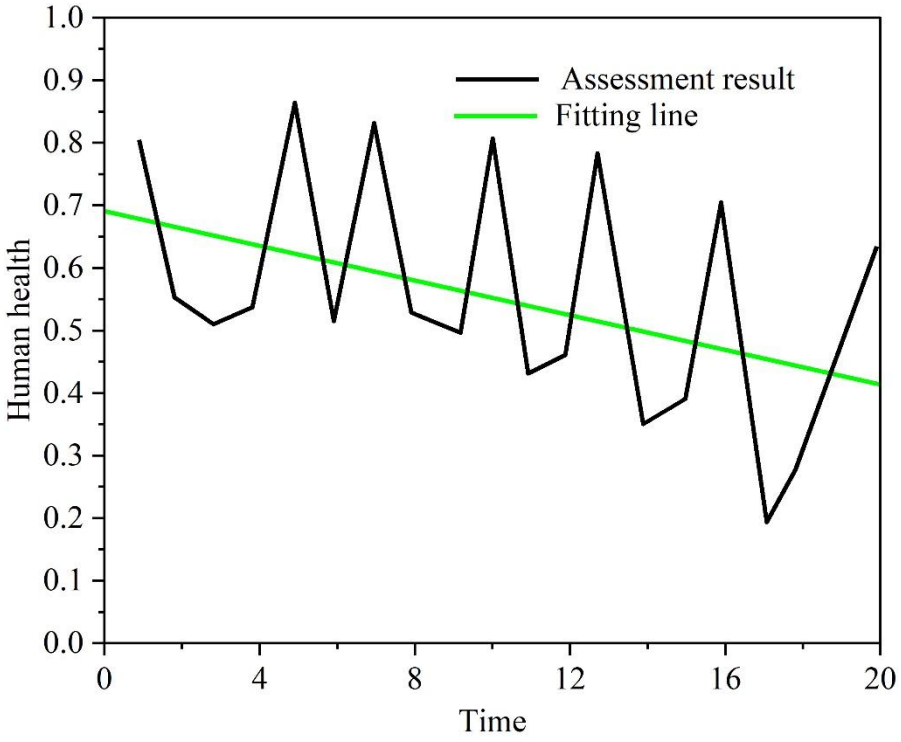

(b) Results based on four normal physiological characteristics

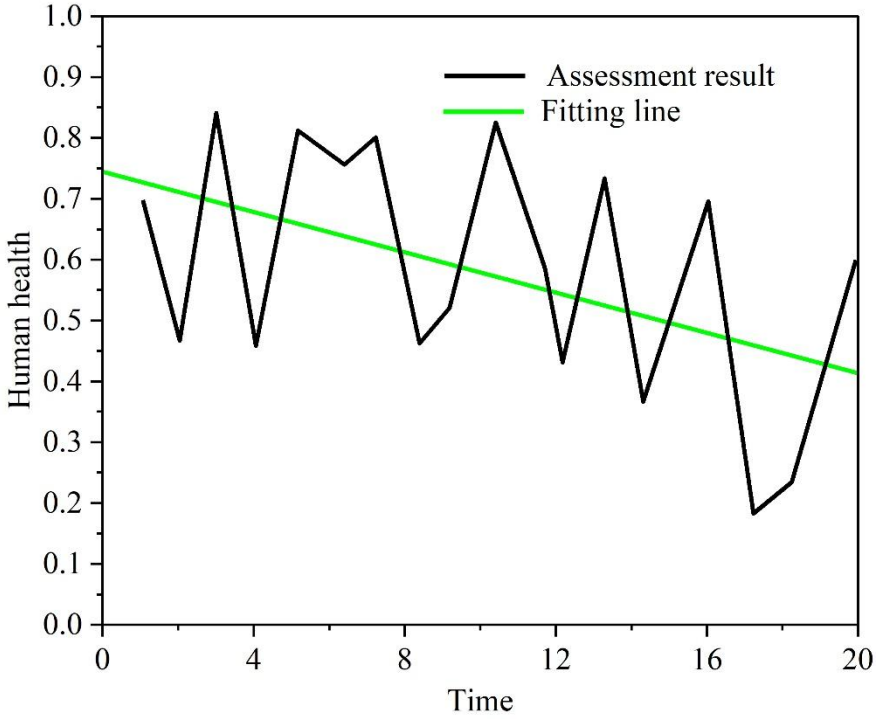

(c) Based on the results of 42 new primitive characteristics

Figure 6. The changes in human health.

To further validate the accuracy of the results of the HMM-based health assessment, we analyzed a second set of data. The test subject was a 23-year-old active athlete and the entire test period was 15 days. During the test, the 23-year-old active athlete had no discomfort and maintained good health. The 42 fusion feature matrices corresponding to the two testers were firstly mapped to the 3-dimensional space respectively, and the results are shown in Figure 7.

From the figure, it can be found that after the two sets of data have been downscaled, only a small part of the feature data overlap with each other in the 3-dimensional space, of which the large part is separated from each other. Through the method of dimensionality reduction, we can distinguish the results of different people's health status to a certain extent.

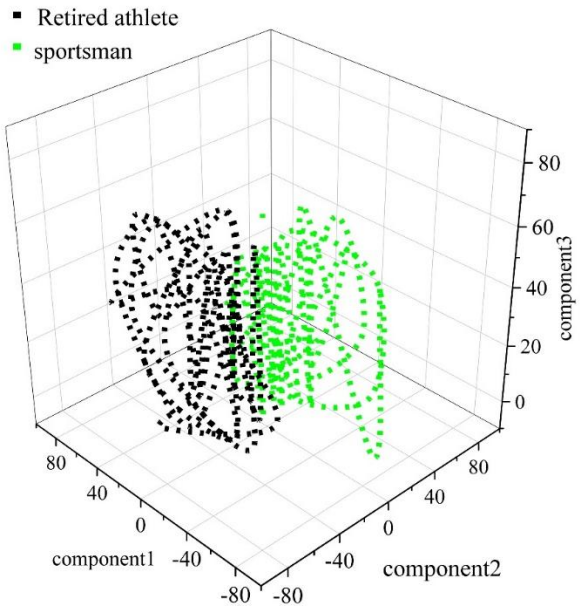

Figure 7. The feature matrix maps the results.

In order to further distinguish the health status between the two, we imported the 2 sets of dimensionality reduced feature data into the HMM, selected the first day data of the testers as the training samples, the basic parameters were set: the implied state was 2, the number of mixed Gaussian functions was 3, and the results of the health assessment based on the 42 features are shown in Fig. 8. Figure (a) shows the results for a 23-year-old active athlete and Figure (b) shows the final assessment results for a 30-year-old retired athlete. For Fig. (a), the fitted curve rises from 0.410 to 0.475, and the overall trend rises by 0.065 with almost no change, while their actual physical condition remains good and there is no health risk. The experimental results prove the rationality as well as the accuracy of the HMM-based health risk assessment model for athletes established in this paper.

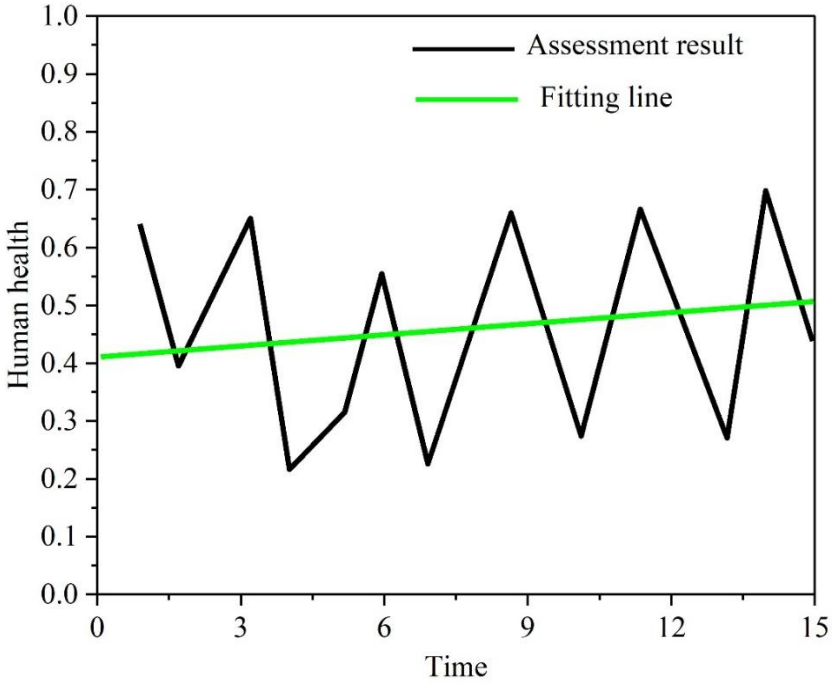

(a) The result of the 23 year old active athlete

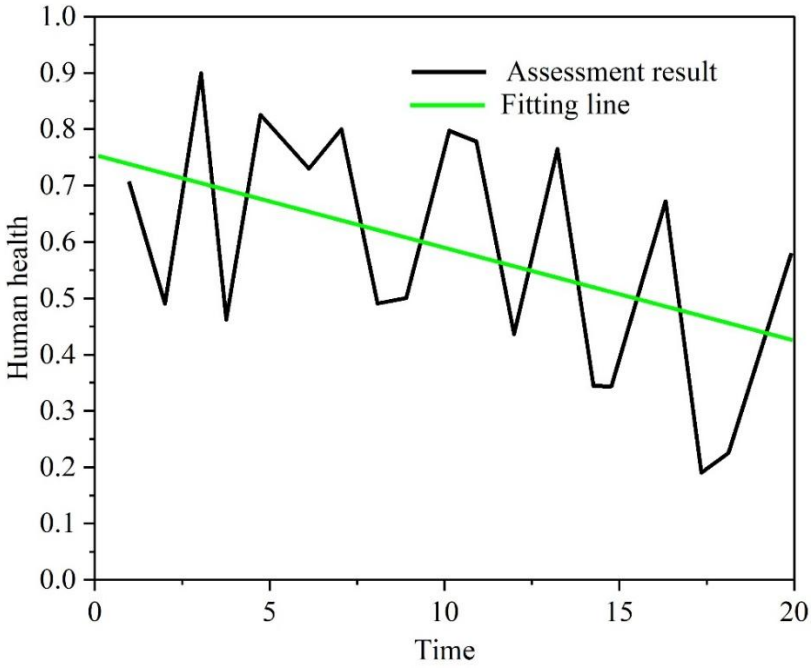

(b) Final assessment of retired athletes at the age of 30

Figure 8. Health assessment results.

6. Conclusion

In this study, we designed a pulse wave-based health status monitoring system for athletes to propose a health risk assessment model for athletes based on the Hidden Markov Model.

The results of pulse signal feature parameter extraction showed that the marginal spectral frequencies of healthy people were concentrated between 0 and 11 Hz, and the marginal spectral energies of patients with coronary heart disease were still distributed above 11 Hz, and the marginal spectral frequencies of healthy people were more concentrated. The mean squared deviation of IMF energy of healthy people is lower than 17, while the mean squared deviation of IMF energy of patients with coronary heart disease is more than 20 and reaches 28.3795. The difference of pulse signal characteristic parameters of people with two different health statuses suggests that the method of pulse characteristic parameter extraction proposed in this paper is of practical significance for the monitoring of the athletes' health status, which can promote the scientific and healthy development of the sports industry. It can promote the scientific and healthy development of sports.

Based on the Hidden Markov Model, the health risk assessment model of athletes can further utilize the physiological data of athletes collected by the detection system to effectively distinguish the difference in health status between 30-year-old retired athletes and 23-year-old active athletes. The fitted curve of the physical health level of the identified healthy athletes increased by 0.065 as a whole, with a better actual physical condition and a good health risk assessment status. It confirms that the model in this paper can accurately predict the ecological health level of athletes, reveal their existing health risks, and win valuable preventive time for the protection of their physical health.

References

1. Leonardi, F. (2018). The definition of health: towards new perspectives. *International Journal of Health Services*, 48(4), 735-748.
2. Malm, C., Jakobsson, J., & Isaksson, A. (2019). Physical activity and sports—real health benefits: a review with insight into the public health of Sweden. Sports, 7(5), 127.
3. Chu, T. (2021). The influence of sports on health science and its factors. Revista Brasileira de Medicina do Esporte, 27(3), 327-330.
4. Lee, E. C., Fragala, M. S., Kavouras, S. A., Queen, R. M., Pryor, J. L., & Casa, D. J. (2017). Biomarkers in sports and exercise: tracking health, performance, and recovery in athletes. The Journal of Strength & Conditioning Research, 31(10), 2920-2937.
5. Runacres, A., Mackintosh, K. A., & McNarry, M. A. (2021). Health consequences of an elite sporting career: long-term detriment or long-term gain? A meta-analysis of 165,000 former athletes. Sports Medicine, 51, 289-301.
6. Fagher, K., Badenhorst, M., Kunorozva, L., Derman, W., & Lexell, J. (2023). "It gives me a wake up call"—It is time to implement athlete health monitoring within the Para sport context. Scandinavian Journal of Medicine & Science in Sports, 33(5), 776-786.
7. Jimenez, C., & Verhagen, E. (2025). Reimagining athlete monitoring for true indicative injury prevention. BMJ Open Sport & Exercise Medicine, 11(2).
8. Kraus, E., Tenforde, A. S., Nattiv, A., Sainani, K. L., Kussman, A., Deakins-Roche, M., ... & Fredericson, M. (2019). Bone stress injuries in male distance runners: higher modified Female Athlete Triad Cumulative Risk Assessment scores predict increased rates of injury. British journal of sports medicine, 53(4), 237-242.
9. Hull, J. H., Jackson, A. R., Ranson, C., Brown, F., Wootten, M., & Loosemore, M. (2021). The benefits of a systematic assessment of respiratory health in illness-susceptible athletes. European Respiratory Journal, 57(6).
10. Gabbett, T. J., Nassis, G. P., Oetter, E., Pretorius, J., Johnston, N., Medina, D., ... & Ryan, A. (2017). The athlete monitoring cycle: a practical guide to interpreting and applying training monitoring data. British journal of sports medicine, 51(20), 1451-1452.
11. Narzullaev, D., Tursunov, A., Samigova, N., Tursunov, U., & Shadmanov, K. (2021). Methods for assessing risk factors to the health of highly qualified athletes. In E3S Web of Conferences (Vol. 284, p. 01010). EDP Sciences.
12. Islam, N. N., Khan, N. I., Razzak, M. A., & Islam, M. N. (2021, November). Design, development, and evaluation of a physical exercise monitoring and managing system for athletes. In The 23rd International Conference on Information Integration and Web Intelligence (pp. 443-451).
13. Kaur, A., Kaur, R., & Jagdev, G. (2021). Analyzing and exploring the impact of big data analytics in sports sector. SN Computer Science, 2(3), 184.
14. Mou, C., & Cheng, Y. (2021). Research on information resource sharing and big data of sports industry in the background of OpenStack cloud platform. Security and communication networks, 2021(1), 2824146.
15. Patel, D., Shah, D., & Shah, M. (2020). The intertwine of brain and body: a quantitative analysis on how big data influences the system of sports. Annals of Data Science, 7(1), 1-16.
16. Eid, A. I. A., Miled, A. B., Fatnassi, A., Nawaz, M. A., Mahmoud, A. F., Abdalla, F. A., ... & Mohamed, I. B. (2024). Sports prediction model through cloud computing and big data based on artificial intelligence method. Journal of Intelligent Learning Systems and Applications, 16(2), 53-79.

17. Chao, Z., Yi, L., Min, L., & Long, Y. Y. (2024). IoT-Enabled Prediction Model for Health Monitoring of College Students in Sports Using Big Data Analytics and Convolutional Neural Network. Mobile Networks and Applications, 1-18.
18. Onks, C., Hall, D., Ridder, T., Idriss, Z., Andrie, J., & Narayanan, R. (2021). The accuracy and predictability of micro Doppler radar signature projection algorithm measuring functional movement in NCAA athletes. Gait & posture, 85, 96-102.
19. Goes, F. R., Meerhoff, L. A., Bueno, M. J. O., Rodrigues, D. M., Moura, F. A., Brink, M. S., ... & Lemmink, K. A. P. M. (2021). Unlocking the potential of big data to support tactical performance analysis in professional soccer: A systematic review. European Journal of Sport Science, 21(4), 481-496.
20. Shi, X., & Zou, H. (2024). Data Collection and Analysis based on Sensor Technology in Sports Training. Scalable Computing: Practice and Experience, 25(5), 4399-4406.
21. Kim, K. R., Kang, T. W., Kim, H., Lee, Y. J., Lee, S. H., Yi, H., ... & Yeo, W. H. (2024). All-in-One, Wireless, Multi-Sensor Integrated Athlete Health Monitor for Real-Time Continuous Detection of Dehydration and Physiological Stress. Advanced Science, 11(33), 2403238.
22. Hu, Y., & Liu, J. (2024, August). Real-Time Monitoring and Early Warning System of Athlete Health Condition Based on Computer Internet of Things. In 2024 IEEE 2nd International Conference on Sensors, Electronics and Computer Engineering (ICSECE) (pp. 1392-1398). IEEE.
23. Sekeroglu, M. O., Pekgor, M., Algin, A., Toros, T., Serin, E., Uzun, M., ... & Ermis, S. A. (2025). Transdisciplinary Innovations in Athlete Health: 3D-Printable Wearable Sensors for Health Monitoring and Sports Psychology. Sensors, 25(5), 1453.
24. Lebedev, G., Gureeva, A., & Tikhonova, Y. (2017). Software system for dynamic athlete health monitoring. Procedia computer science, 112, 1664-1669.
25. Leduc, C., & Weaving, D. (2025). Invisible Monitoring for Athlete Health and Performance: A Call for a Better Conceptualization and Practical Recommendations. International Journal of Sports Physiology and Performance, 1(aop), 1-5.
26. Koltun, K. J., Strock, N. C., Southmayd, E. A., Oneglia, A. P., Williams, N. I., & De Souza, M. J. (2019). Comparison of Female Athlete Triad Coalition and RED-S risk assessment tools. Journal of sports sciences, 37(21), 2433-2442.
27. Iduh, B. N., Umeh, M. N., Anusiuba, O. I., & Egba, F. A. (2024). Development of a Predictive Modeling Framework for Athlete Injury Risk Assessment and Prevention: A Machine Learning Approach. European Journal of Theoretical and Applied Sciences, 2(4), 894-906.
28. Difeng Sun,He Xu,Zutang Wu,Jin Li,Youcao Wu & Jianbing Li. (2025). Logarithm Radon-Fourier transform for high speed small target detection with atmospheric resistance effect. Digital Signal Processing,165,105335-105335.
29. Yan Zhao,Pei Yao & Liang Xue. (2025). Image steganography based on wavelet transform and Generative Adversarial Networks. Journal of Visual Communication and Image Representation,110,104474-104474.
30. Haosu Zhang,Liang Yang,Lei Zhang,Yong Du,Chaoqi Chen,Wei Mu & Lingji Xu. (2025). An Electro-Magnetic Log (EML) Integrated Navigation Algorithm Based on Hidden Markov Model (HMM) and Cross-Noise Linear Kalman Filter. Sensors,25(4),1015-1015.